

# The potential of ~~InSAR~~ synthetic aperture radar interferometry for assessing meltwater lake dynamics on Antarctic ice shelves

Weiran Li <sup>1</sup>, Stef Lhermitte <sup>1</sup>, and Paco López-Dekker <sup>1</sup>

<sup>1</sup>Department of Geoscience and Remote Sensing, Delft University of Technology, Delft, The Netherlands

**Correspondence:** Weiran Li (w.li-7@tudelft.nl)

**Abstract.** Surface meltwater drains on several Antarctic ice shelves, resulting in surface and sub-surface lakes that are potentially critical for the ice shelf collapse. ~~Yet~~ Despite these phenomena, our understanding and assessment of the drainage ~~or~~ and refreezing of these lakes is limited, mainly due to lack of field observations and to the limitations of optical satellite imagery during polar night and in cloudy conditions. Therefore, this paper explores the potential of backscatter intensity and of interferometric coherence and phase from C-band synthetic aperture radar (SAR) imagery as an alternative to assess the dynamics of meltwater lakes. In ~~two case studies~~ four case study regions over Amery and Roi Baudouin ice shelves, ~~we analyse i) the spatial and ii) the temporal variations of~~ East Antarctica, we examine spatial and temporal variations in SAR backscatter intensity ~~with iii) coherence and iv) interferogram phase and interferometric~~ (InSAR) ~~patterns detected by Sentinel-1 data over multiple meltwater lakes~~ coherence and phase over several lakes derived from Sentinel-1A/B C-band SAR imagery. Throughout the year, the lakes are observed in completely frozen state, in partially frozen state with a floating ice lid, and as open water lakes. ~~The~~ Our analysis reveals that the meltwater lake delineation is challenging during the melting period when the contrast between melting snow and lakes is ~~confounded. On the other hand, it shows that the~~ indistinguishable. Despite this finding, we show using a combination of backscatter and InSAR observations that lake dynamics can be effectively captured during ~~the refreezing process and the winter season by combining backscatter and InSAR information. In particular, the InSAR coherence and interferogram phase information are deemed essential throughout this whole period to distinguish~~ other non-summertime months. Moreover, our findings highlight the utility of InSAR-based observations for discriminating between refrozen ice and subsurface meltwater, and indicate the potential for phase-based detection and monitoring of rapid meltwater drainage events. ~~Additionally, the results provide significant evidence on the potential of the interferogram fringe patterns to detect and characterise instant events, such as lake drainage events over ice shelves.~~ The potential of this technique to monitor these meltwater change events is ~~however,~~ however, strongly determined by the satellite revisit interval and potential changes in scattering properties due to snowfall or melt events.

## 1 Introduction

~~Over the past decades, widespread~~ Widespread surface meltwater has been ~~spotted over multiple ice shelves in Antarctica (Kingslake et al., 2017) with potential far-reaching implications for hydrofracturing and ice shelf collapse (Bell et al., 2018)~~ Since meltwater lakes and ponds increase the gravitational load, depressing the ice shelf surface and inducing an upliftin

the surrounding, the stress in the uplifting area can lead to fracture. On the contrary, a draining meltwater pond leads to a hydrostatic rebound, which also results in fracture (Banwell et al., 2013). The repeating filling and drainage process increases the vulnerability of the ice shelf to hydrofracture observed on Antarctic ice shelves over the past century (Kingslake et al., 2017). Through seasonal formation and draining of supraglacial lakes, which have the potential to fracture and weaken ice shelves through repeated compression and uplift, respectively (Banwell et al., 2013), such phenomena may have important implications for ice-shelf hydrofracture and collapse (Bell et al., 2018). Therefore, assessing the accurately observing the spatial and temporal evolution (filling, drainage or refreezing of these lakes on Antaretic ice shelves is key to understanding the response of Antaretica in a future climate) of such lakes is pertinent to elucidating the future stability and response of the Antarctic Ice Sheet to climate change.

Satellite remote sensing has been the major tool to delineate supra-glacial lakes and assess surface meltwater dynamics, given the Given the remote location, large extent/widespread area, and harsh conditions that limit extensive field observations on Antaretica climatic conditions in which these lakes form, satellite remote sensing has become the primary method of observing their evolution and dynamics (Brucker et al., 2010; Dirscherl et al., 2021). Previous studies exploited various satellite remote sensing data sources, including optical and synthetic aperture radar (SAR) imagery. For to observe these phenomena; for example, Kingslake et al. (2017) provided-presented an overview of the Antarctic-wide meltwater hydrological network by combining Landsat, WorldView and Aster satellite imagery in combination with optical satellite imagery together with historic (pre-satellite) aerial photography. A study from Lenaerts et al. (2016) detected meltwater features on the Other work has combined both optical and synthetic aperture radar (hereafter SAR) imagery to detect meltwater features in both Greenland and Antarctica (Benedek and Willis, 2021; Dirscherl et al., 2021), including the detection of subsurface meltwater across East Antarctica's Roi Baudouin Ice Shelf (RBIS) using a combination of optical Landsat imagery and L-band radar imagery from the ALOS/PALSAR instrument, which is capable of mapping subsurface meltwater. Optical imagery (e.g. Landsat-8) and C-band SAR imagery (e.g. Sentinel-1 in HH and/or HV polarisation) are combined to detect subsurface meltwater in (Miles et al., 2017) and lake drainage in (Benedek and Willis, 2021) in Greenland and Antarctica (Dunmire et al., 2020), whereas Dirscherl et al. (2021) used deep learning techniques on Sentinel-1 HH backscatter intensities for automated supraglacial lake mapping across Antaretica; Lenaerts et al. (2016)). Such subsurface melting is not detectable from optical-based imagery alone (Miles et al., 2017), emphasising the potential utility of SAR to better detect total surface meltwater presence.

Despite the potential of optical imagery and SAR data in detecting and monitoring imagery in observing surface meltwater, both methods/sensor types have limitations over Antarctica. Polar nights and cloud cover limit data availability from visible band and near-infrared imagery (Selmes et al., 2013; Williamson et al., 2017), which is not the case for Sentinel-1 SAR data. The, for example, limit data coverage in optical-based imagery (Williamson et al., 2017), whereas the operating frequencies and active-source configuration of SAR sensors allow for all-weather, day-night imaging (Miles et al., 2017). Relative to intuitive representation of meltwater features detected by optical sensors, however, the interpretation of SAR imagery can be complex due to ambiguous backscatter returns and/or image geometry effects (e.g. Fahnestock et al. (1993); Miles et al. (20)). While cross-polarised backscatter intensity (HV or VH) provides on average backscatter intensity SAR images generally provide a better contrast between water and ice than HH polarisation (Miles et al., 2017), but it is not single polarisation (e.g.

HH images (Miles et al., 2017), such images are not necessarily always available over Antarctica. ~~Interpreting radar imagery moreover may not be that straightforward as snow (Fahnestock et al., 1993) and meltwater features (Miles et al., 2017) in SAR images can result in ambiguous signals. (Hillebrand et al., 2021).~~

65 The ambiguity in meltwater lake features SAR imagery is the result of the combination of dielectric properties and geometry, which both determine the backscatter intensity and which can be related to multiple factors including wetness, roughness and snow grain size (Fahnestock et al., 1993). For example, both dry snow and bare ice typically show low backscatter intensities due to limited volume scattering and specular reflection over the blue ice area. A melting snow/firn surface or open lake, however, also results in low backscatter intensities due to the increased absorption due to change in dielectric constant (Ulaby et al., 1981; Nagler et al., 2016). Refrozen snow/firn with large snow grains, on the other hand, result in strong  
70 backscatter intensities due to the high volume scattering (Fahnestock et al., 1993), but can be easily confounded with rough surfaces or ice lids that also result in high backscatter intensities due to the roughness or the high dielectric contrast between the ice lid and water below (Hirose et al., 2008; Antonova et al., 2016). The meltwater features may moreover change over time resulting in variable backscatter intensity signatures. Complete refreezing of a lake, for example, may result in the disappearance of the high dielectric contrast between the ice lid and water below, resulting in a decrease in backscatter intensity  
75 (Hirose et al., 2008).

A potential solution to these limitations is interferometric processing of the synthetic aperture radar data (InSAR), which provides complementary information on the geometric and dielectric properties of the meltwater features. Repeat-pass InSAR method processes pairs of images of the same area separated by a ~~certain time~~ particular temporal baseline to derive coherence and interferometric phase information. ~~The coherence can be considered as an indicator for~~ Coherence is considered an  
80 indicator of changes in the relative position of the scatterers between the two acquisitions, whereas the interferometric phase measures their ~~average~~ range difference from the satellites with the precision of the whole or a fractional component of the measuring radar wavelength. For high coherence areas, the phase can be related to a line-of-sight displacement without change in scattering properties (~~e.g. without intense regional precipitation and melts~~), whereas for low coherence areas where surface melts typically occur, the phase becomes scarcely informative (Hanssen, 2001). ~~This~~ We expect this combination of coherence  
85 and phase information from InSAR ~~is expected~~ to facilitate the continuous monitoring of meltwater dynamics. ~~For example, in absence of changes in scattering due to changing snow/ice conditions or intense regional melts, the coherence of the InSAR images should be generally high. However, when lakes drain or refreeze, the scattering properties will change, reducing the coherence of the InSAR images. These changes in InSAR coherence~~ The changes in InSAR coherence have been proven useful in X-band for monitoring the refreeze of thermokarst lakes in the Arctic region (Antonova et al., 2016). So far, however, no  
90 analysis has been conducted for C-band ~~time-series~~ time series. Additionally, the interferometric phase might reveal information about the drainage and filling of lakes, as these processes ~~basically~~ result in a vertical displacement of the surface (Banwell et al., 2013). However, the ~~added value of~~ value added using InSAR for such applications has not ~~been tested or quantified yet~~ yet been examined.

~~The objective of this paper is to~~ In this paper, we assess the potential of C-band InSAR data to quantify the dynamic behaviour  
95 of meltwater filling, drainage and refreezing. For this purpose, we use a combination of backscatter ~~intensities and InSAR~~

information from the Sentinel-1 mission to monitor the meltwater over two Antarctic ice shelves (i.e. Roi Baudouin Ice Shelf, coherence and phase information to monitor recent meltwater features over two East Antarctic locations—the Amery and Roi Baudouin (RBIS) and Amery Ice Shelf (Amery)) as case studies where we have optical satellite ice shelves—using data collected by Sentinel-1A/B in 2017/2018. To supplement the interpretation of our (In)SAR-based analyses, we also utilise spatially and temporally collocated optical and radiometric satellite data and climate data as additional reference data.

## 2 Data & Methods

### 2.1 Study areas

Two ice shelves in East Antarctica with well-known meltwater dynamics (Kingslake et al., 2017) have been used as case studies for this study. The first case study is on the Roi Baudouin Ice Shelf (RBIS), where in situ research has been conducted and the exact locations of several lakes were mapped during a field campaign in Jan./Feb. 2016 (Lenaerts et al., 2016), which were revisited in Nov. 2017 when their lake collapse has been observed (Dunmire et al., 2020). In the RBIS case study, we used the field campaigns (Lenaerts et al., 2016; Dunmire et al., 2020). We use the supraglacial and englacial lakes mapped by Lenaerts et al. (2016) as delineated meltwater lake features and complemented, and complement that data set with manually delineated sample polygons of snow and ice surfaces based on Landsat imagery for studying the difference between meltwater lakes and the solid surrounding regions (Fig. 1).

For the second case study over Amery ice shelf, we used a similar approach based on a sampled lake, snow and ice sample regions. For Amery, however, a reference lake data set was not no previously published dataset from in situ studies is available. Therefore, lakes samples were samples of lakes are mapped manually based on available Landsat-8 imagery in Landsat 8 imagery (introduced in Section 2.2) in summer 2017-2018. The goal of this sampling was is not to map all possible lakes, but to get a representative sample polygon for each snow/ice/lake class. Our lake class, however, overlaps with the lakes as mapped by Spergel et al. (2021).

### 2.2 Data

Two types of Level-1 Sentinel-1 Interferometric Wide (IW) products are used in this study: Single Look Complex (SLC) products, consisting of complex-valued data that preserve the phase information of the returned echoes, and Ground Range Detected (GRD) products, consisting of multi-looked backscatter intensity without phase information. GRD products are used mainly as supplementary backscatter intensity information when specific SLC tracks are not available (data specification and availability are described in Table 1). For both products, HH-polarisation was is used as this is the only polarisation widely available over Antarctica the studied ice shelves. The GRD data were downloaded from the are acquired from Google Earth Engine (GEE), whose processing includes thermal noise removal, radiometric calibration, and terrain correction. The final backscatter product has a 20 m×20 m resolution. When normalised by the area of the resolution cell on the ground, the

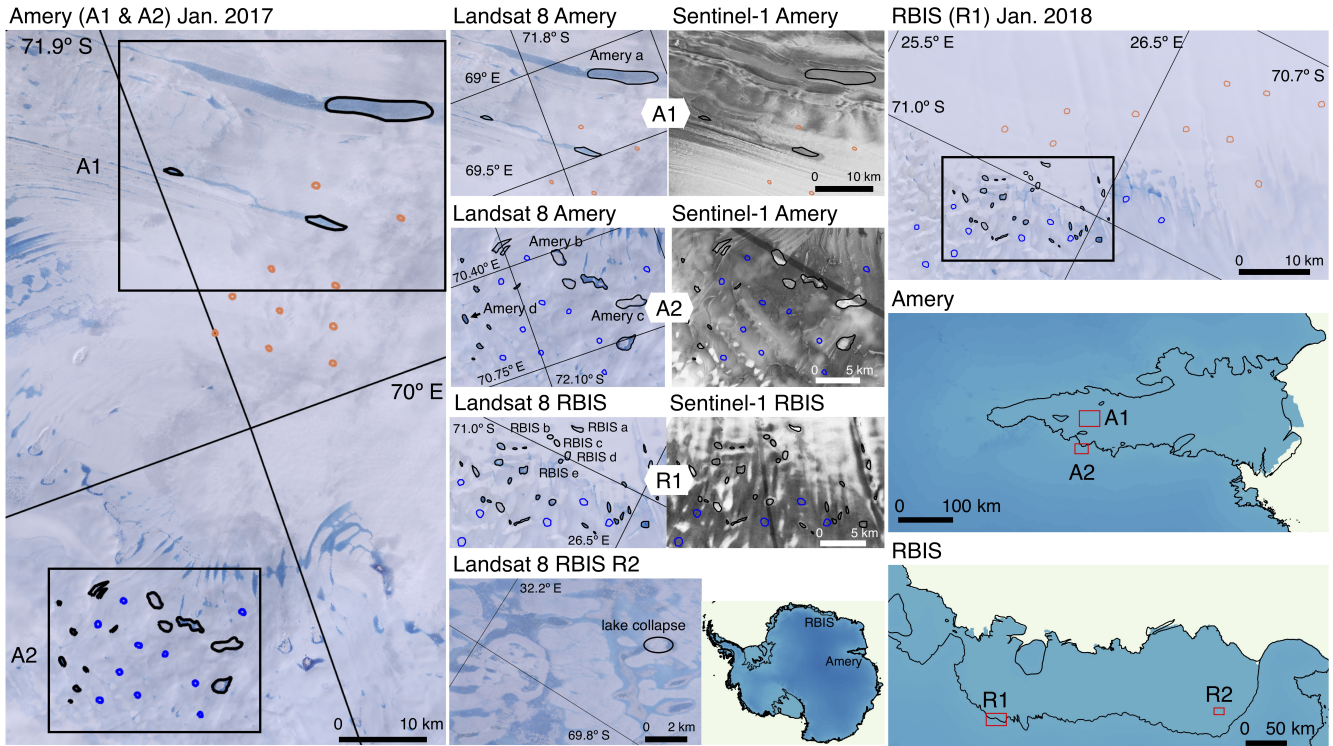


**Figure 1.** Outline of the Amery and Roi Baudouin Ice Shelf (RBIS) study areas (referred to as A1, A2, R1, and R2). Close-ups-Details of the investigated meltwater features are shown in both Landsat 8 RGB images and Sentinel-1 backscatter intensities. In all panels, the lakes used for the temporal backscatter and coherence analysis are delineated in-as black curves. The indices-labels of the lakes correspond to the time series in Fig. 3. Snow (in orange) and ice (in blue) are also delineated as-comparison for comparison-against backscatter intensities-intensity and coherence values-observed-over-lakes (Fig. Figure 3). Panel R2 illustrates the lake feature selected-for-the-interferogram-analysis shown in Fig. Figure 9. The analysed locations-ice-shelves are highlighted in the Antarctica map, and-the-specific-locations-of-A1, A2, R1 and R2 are shown in the Amery and RBIS maps. The DEM used as the background is from the REMA project (Howat et al., 2019), courtesy-of-the-Polar-Geospatial-Center. The coastline is from the SCAR Antarctic Digital Database (Gerrish et al., 2021).

calibrated backscatter intensities are usually recalled as ~~Normalized Radar Cross Sections (NRCS)~~ $\sigma^0$ , and this is the term we will use for the remaining of the paper for backscatter intensity.

The Sentinel-1 SLC data ~~were downloaded from the~~ are available on Copernicus Open Access Hub (?) and (Copernicus, 2014) and are processed to derive phase information and ~~NRCS~~ $\sigma^0$ . SLC processing and georeferencing ~~were is~~ carried out using the Delft Object-oriented Radar Interferometric Software (DORIS), ~~http://doris.tudelft.nl~~, and is illustrated in Fig. 2. The SLC data are read and saved as a specific format for processing (as in Fig. 2). The co-registration between images is performed using magnitude images of the complex data. Sentinel-1 IW operates in Terrain Observation by Progressive Scans (TOPS, De Zan and Monti Guarnieri (2006)) mode, therefore phase ramps are accounted for via deramp and reramp processes to ensure co-registration accuracy (Yague-Martinez et al., 2016). For the retrieval of the sub-pixel azimuth shift, Enhanced Spectral Diversity (ESD) is applied in addition (Prats-Iraola et al., 2012; Yague-Martinez et al., 2017). Georeferencing is based on TanDEM-X digital elevation model (DEM) for RBIS (Lenaerts et al., 2016) and WGS84 geoid for Amery as it is the default DEM input of DORIS when TanDEM-X DEM of the same quality is not available. The final SLC products have an azimuth resolution of 20 m and a ground range resolution of 5 m (Torres et al., 2012).

~~Additionally, Landsat 8 imagery was used as evaluation dataset to help interpreting~~

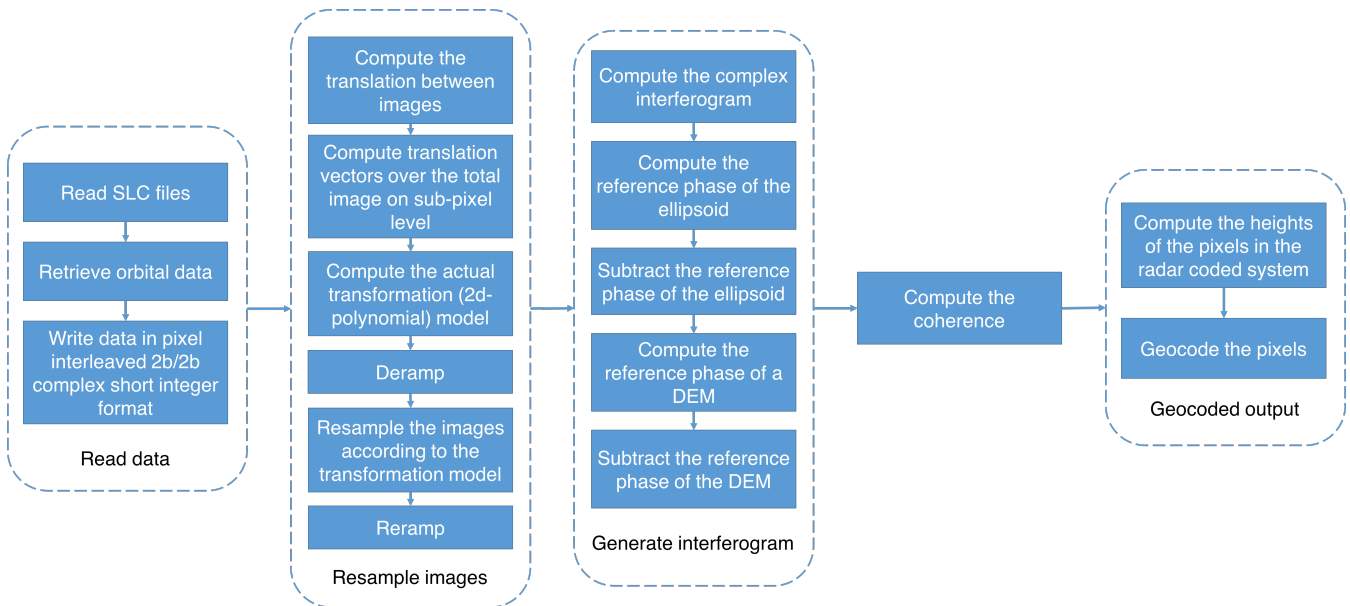


**Figure 2.** Delft Object-oriented Radar Interferometric Software (DORIS) processing flowchart from the software documentation available online at [http://doris.tudelft.nl/software/doris\\_v4.02.pdf](http://doris.tudelft.nl/software/doris_v4.02.pdf), customised based on Nikaein et al. (2021).

140 ~~Additionally, independent datasets are used to help interpret~~ the Sentinel-1 SAR data. ~~For this purpose, available Landsat images were processed on the GEE~~First, Landsat 8 images are used for visual interpretation, i.e. solid snow and ice surfaces are shown in the images in white, and ice and lakes as a result of intensive melt are shown in blue. Available calibrated

**Table 1.** List of the imagery used ~~for the in this~~ study. When the end date is not specified, the table entry refers to a single acquisition. For SLC data from descending track 3, the repeat cycle is mainly 6 days, except that between Jan. 4 and Jan. 16, 2017 the revisit time is 12 days, and there is a lack of data on May 16, Sep. 13 and Sep. 19, 2017. For SLC data from ascending track 59, there is a lack of data on Feb. 26, 2018 and Mar. 10, 2018.

Ice shelf ( <u>region</u> )	Product	Track No.	Starting date	End date	Repeat cycle
RBIS ( <u>R1</u> )	Sentinel-1 IW SLC	Ascending 59	2017/07/25	2018/04/15	12 days
RBIS ( <u>R2</u> )	Sentinel-1 IW SLC	Descending 136	2017/12/04	2018/04/15	12 days
RBIS ( <u>R1</u> )	Sentinel-1 IW GRD	Multiple	2016/06/01	2018/05/31	N/A
RBIS ( <u>R1</u> )	Landsat 8	Path 157 Row 110	2017/09/26	-	N/A
RBIS ( <u>R2</u> )	Landsat 8	Path 155 Row 110	2017/12/01	-	N/A
RBIS ( <u>R2</u> )	Landsat 8	Path 153 Row 110	2017/12/19	-	N/A
RBIS ( <u>R1</u> )	Landsat 8	Path 156 Row 110	2018/01/09	-	N/A
Amery ( <u>A1, A2</u> )	Sentinel-1 IW SLC	Descending 3	2017/01/04	2018/01/17	12 or 6 days
Amery ( <u>A2</u> )	Sentinel-1 IW GRD	Multiple	<del>2015</del> <u>2016/11/06/29-01</u>	2018/05/31	N/A
Amery ( <u>A1</u> )	Landsat 8	Path 127 Row 111	2017/01/27	-	N/A
Amery ( <u>A2</u> )	Landsat 8	Path 126 Row 111	2017/10/03	-	N/A
Amery ( <u>A1, A2</u> )	Landsat 8	Path 127 Row 111	2018/01/14	-	N/A

top-of-atmosphere (TOA) Tier 1 Landsat surface reflectance data (Chander et al., 2009) of RGB (bands 4, 3, and 2) and panchromatic (band 8) bands are acquired from GEE at their native 30 m pixel resolution without any additional pre-processing steps. Detailed data type and acquisition dates of satellite imagery are provided in Table 1.

To interpret temporal variations of Sentinel-1 backscatter intensity and coherence, it is moreover important to understand temporal melt extent and precipitation, as these are the potential drivers of changes in scatterers. For estimating melt extent, multi-frequency radiometer observations, more specifically, brightness temperature ( $T_b$ ) measurements from the Special Sensor Microwave Imager/Sounder (SSMIS) sensors (Kunee et al., 2008) are used.

Precipitation from ERA5 Daily Aggregates (Copernicus Climate Change Service (C3S), 2017) over A2 and R1 (in Fig. 1) in 5 km resolution is averaged spatially and acquired from GEE. Acquisition dates of the brightness temperature observations and ERA5 data overlap with the SLC acquisition dates from ascending track 59 and descending track 3 in Table 1.

### 2.3 Methods

~~To assess the potential of SAR backscatter intensities and InSAR coherence and phase for assessing~~ To assess meltwater lake dynamics, we analyse the spatial and the temporal variations of Sentinel-1 backscatter intensity and coherence over the lakes and control (snow/ice) sites. Therefore, we compare the spatial and temporal characteristics of the identified lakes with their surroundings to assess how well they can be distinguished in different seasons. For this purpose, the temporal variations in NRCS are first  $\sigma^0$  and coherence are compared per lake, snow, ice class ~~and for the individual lakes.~~ by analysing their time

series of the mean and standard deviation for each class (i.e. lakes, snow and ice). In this comparison, 10 samples of snow and 10 samples of ice on each ice shelf are used as shown in Fig. 1. Second, the spatio-temporal variation in NRCS  $\sigma^0$  is analysed along ~~mono-dimensional~~ cross-sectional transects across the largest lake dimension to assess the seasonal differences between the lakes and their surrounding areas. ~~Subsequently, the NRCS changes~~ This is a biennial analysis, in order to show that the lakes may not behave identically every year. Subsequently, individual images are analysed, where changes in  $\sigma^0$  are compared to changes in coherence and phase to assess the added value of combining ~~NRCS, coherence and phase~~ SAR backscatter intensity with InSAR information to improve the understanding of the melt-refreeze process of lakes.

Time series of backscatter intensity and coherence are interpreted with the assistance of melt extent and precipitation time series. As an approximation of melt extent, the Cross Polarisation Gradient Ratio (XPGR) meltwater detection method proposed by Abdalati and Steffen (1995) is applied, where horizontally polarised 19 GHz (19H) and vertically polarised 37 GHz (37V) brightness temperatures are used to calculate the XPGR:

$$XPGR = \frac{Tb_{19H} - Tb_{37V}}{Tb_{19H} + Tb_{37V}} \quad (1)$$

When XPGR ratio exceeds a specific threshold, the surface is assumed to experience melting. For SSMIS, this threshold is set as -0.0158 (Johnson et al., 2020). 19H and 37V observations used for the computation are measured daily and provided in 25 km resolution. In addition, time series of precipitation from ERA5 acquired from GEE are used directly.

### 3 Results

#### 3.1 Backscatter intensity analysis

The ~~NRCS mean  $\sigma^0$~~  time series of ~~the~~ lakes, snow and ice ~~polygons show a strong seasonal variation, as the local snow~~ (Section 2.2) display strong seasonal variability, consistent with the changing nature of both surface snow and ice properties and the ~~status of the lakes change over~~ evolution of supraglacial lakes through time (Fig. 3). ~~The results on Amery ice shelf show that the NRCS decreases from~~ On Amery Ice Shelf, our observations reveal that  $\sigma^0$  has different levels for snow ( $\sim 0$  dB) to lakes ( $\sim -5$  dB) and ice ( $\sim -10$  dB) ~~during fall, winter, spring, and is relatively constant during the observed time span~~ (fluctuations within  $\sim 1$  dB), with the exception of the summer melt ~~season~~ seasons (January and February) ~~when the NRCS~~. In summer seasons, as a result of melting, the  $\sigma^0$  of (wet) snow and lakes shows a strong drop ~~in NRCS~~ due to the change in dielectric constant ~~as a result of melting~~. The individual highlighted lakes (Amery a, Amery b and Amery d) show slightly different temporal behaviour with drops in NRCS during the melt season, followed by NRCS increase after the melting season. For Amery a and Amery d this increase results in a temporary overshoot until reaching the winter NRCS level again.

The ~~NRCS~~. The  $\sigma^0$  time series on RBIS show a similar pattern (i.e.,  $NRCS_{snow} > NRCS_{lake} > NRCS_{ice}$  between Feb. and Dec.  $\sigma_{snow}^0 > \sigma_{lake}^0 > \sigma_{ice}^0$ ) except for Dec. 2017 and Jan. 2018, where the  $NRCS_{snow}$  drops below the  $NRCS_{lake}$  and  $NRCS_{ice}$ . Some individual lakes also show a different behaviour than the mean lake time series. Lakes RBIS a, for example, which is located in a snow/firn area, shows a high backscatter between July and Dec. 2017 (similar to snow), but subsequently



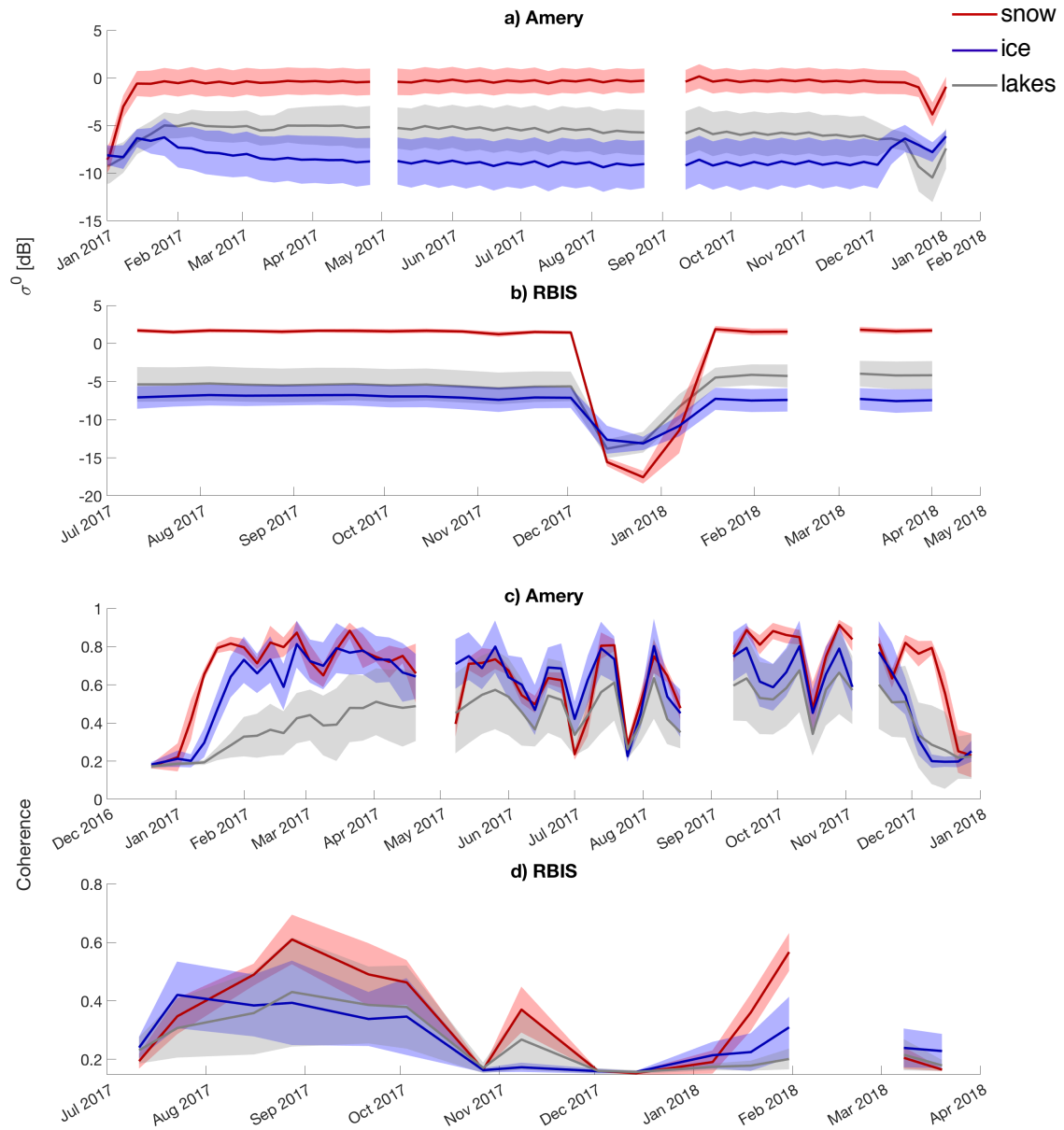


**Figure 3.** Time series of mean (solid line) and standard deviation (semi-transparent area) of NRCS- $\sigma^0$  and coherence over selected polygons—Amery and RBIS—Roi Baudouin ice shelves in—(see Fig. 1 for locations). Moments—Mean and standard deviation are calculated for all features presented. Times with a lack of 6/12-day revisit frequency are masked, resulting in discontinuities.

190 only recovers slowly, while the RBIS f and g show a temporal NRCS behaviour that more closely resembles the ice class.  $\sigma_{snow}^0$  drops below  $\sigma_{lake}^0$  and  $\sigma_{ice}^0$ . Both the Amery and RBIS time series show ~~however~~, however, that the discrimination of lakes based NRCS on  $\sigma^0$  alone is not straightforward as the NRCS  $\sigma^0$  of the lakes often resembles the NRCS  $\sigma^0$  of snow and ice.

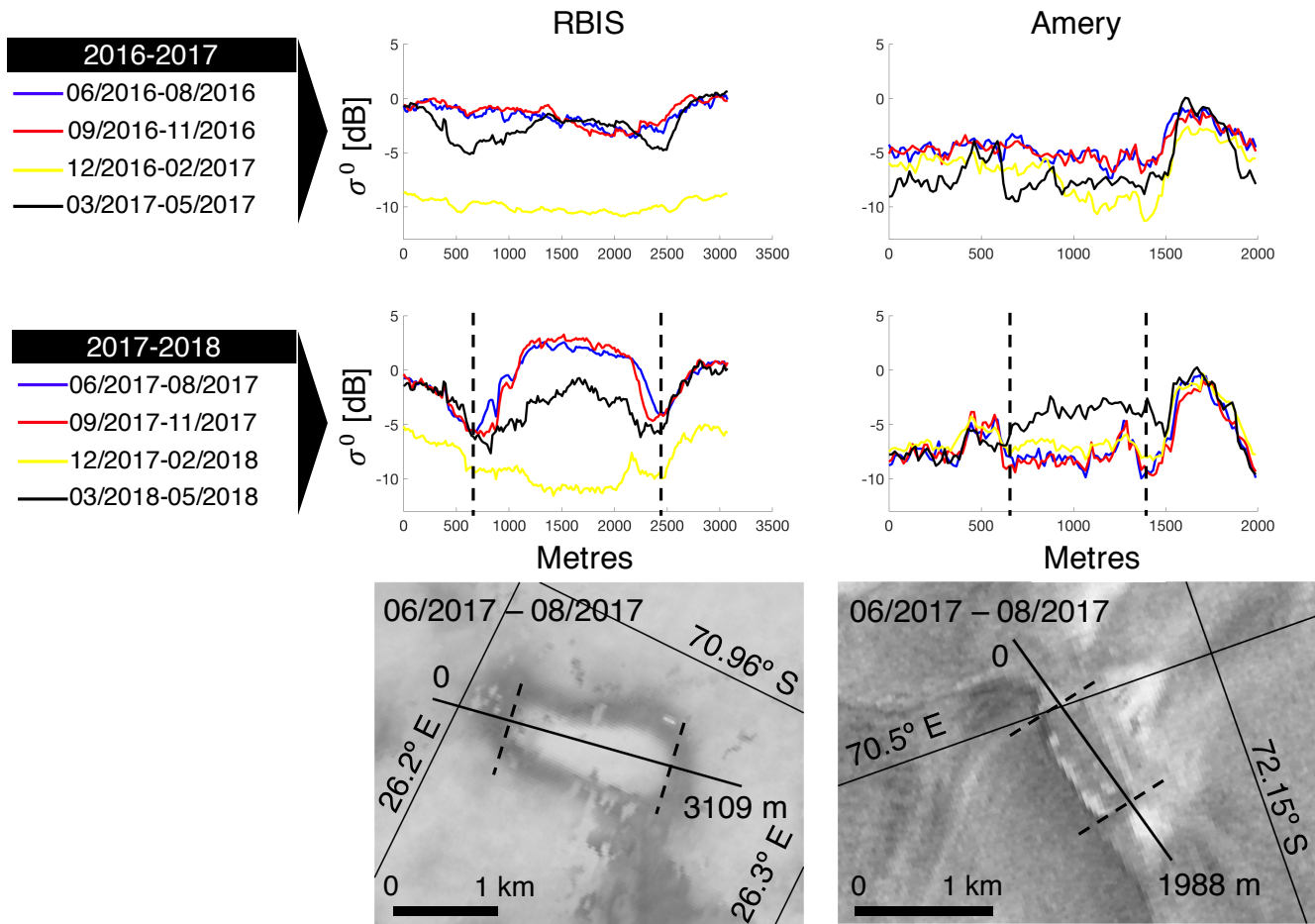


**Figure 4.** Spatial variation of Sentinel-1 NRCS- $\sigma^0$  for two different lakes: RBIS a (see Fig. 1) on the left and Amery d on the right. The upper and middle panels show the mean backscatter intensities over the lake transect for the June 2016 to May 2017 and for the June 2017 to May 2018 periods respectively. Each curve represents the average NRCS- $\sigma^0$  over a quarter year acquisitions. The transects as well as the 2D winter appearance of the feature surroundings are illustrated in the bottom panels.

195 A similar confusion between lakes and snow/ice samples is visible in the spatio-temporal analysis of ~~the transects~~. Both the selected cross-sectional transects. In the case of both RBIS a and Amery d transect (location shown in Fig. 1), for example, backscatter time series show again a significant inter-annual variation (Fig. 4). For RBIS a, this starts with high NRCS- $\sigma^0$

values (similar to snow) with limited spatial variation in ~~June–Nov~~ June–Nov. 2016, followed by a strong ~~area-wide decrease in NRCS~~ area-wide decrease in  $\sigma^0$  during the melting season (Dec. ~~2016–Feb~~ 2016–Feb. 2017). ~~After this~~ Subsequently, a clear spatial pattern emerges with borders of low ~~NRCS and inner areas of high NRCS~~,  $\sigma^0$  at the edges and high  $\sigma^0$  in the 200 central regions, which respectively refer to the edge and central regions of the lake. This pattern is followed again by a new ~~area-wide decrease in NRCS~~ area-wide decrease in  $\sigma^0$  in the Dec. ~~2017–Jan~~ 2017–Jan. 2018 melting season. This development is consistent with the description of ice lids in (Antonova et al., 2016) and the potential development of ice lids in winter on RBIS (Dunmire et al., 2020).

For Amery d, these spatio-temporal transect patterns of the ~~lakes~~ lake are less distinguishable from the ~~ice area surroundings~~ as the NRCS surrounding ice area, as the  $\sigma^0$  of the lake 205 closely resembles the NRCS  $\sigma^0$  of the surrounding ice, except for Mar. ~~May~~ May 2018 when it shows a strong increase.

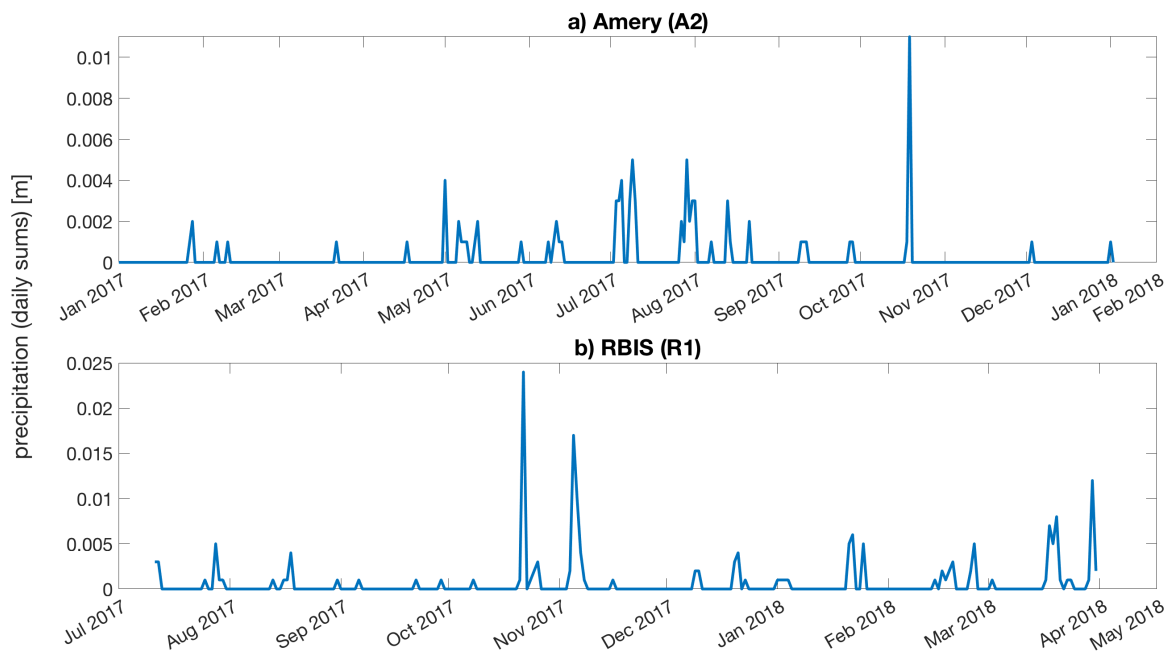


**Figure 5.** ~~Synoptic outline for two lakes of interest on the Amery (referred to as Amery b~~ Precipitation time series spatially averaged over regions A2 and e). ~~The NRCS, the coherence and the associated interferograms are R1 (shown for four representative dates throughout the~~ The fringes in the background of the interferograms show the ice velocity and may indicate tidal movement Fig. Two Landsat images are also shown to aid the visual interpretation of the radar features 1) from ERA5.

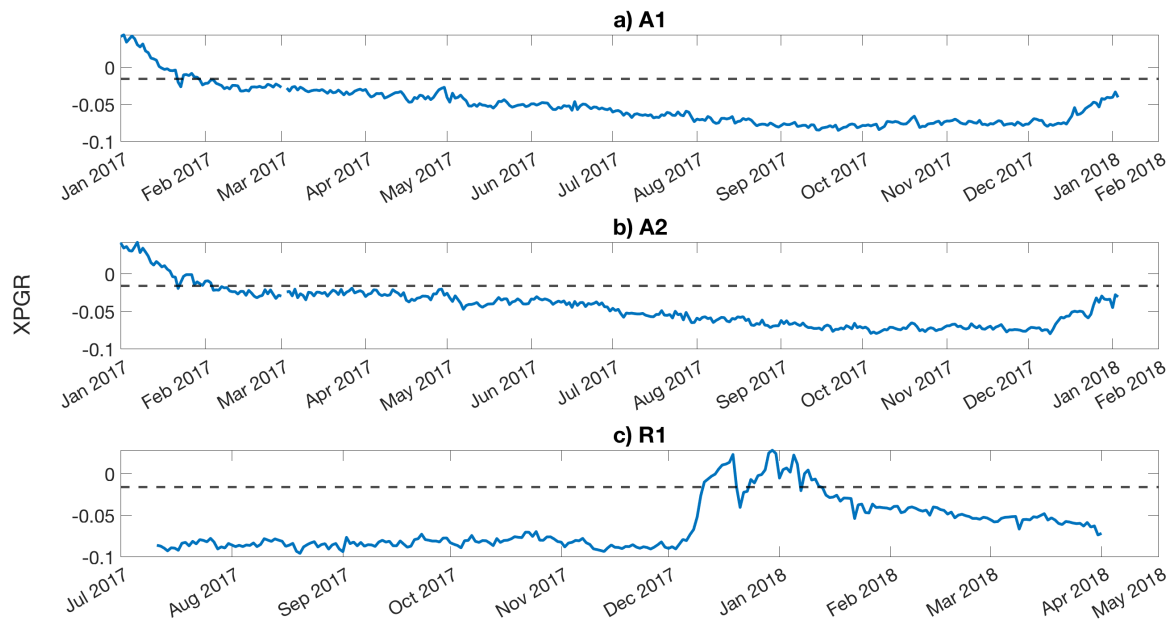


**Figure 6.** Coherence-XPGR time series calculated with Eq. 1 over regions A1, A2 and NRCS in the RBIS region right before R1 (left panels) and during (centre panels) the surface melt shown in the vicinity of RBIS a in the panels (c) of Fig. 1). These lakes are hereby referred to as RBIS a to e. This time series is an approximation of melt extent time series. Two cloud-free Landsat images close to the threshold above which the radar acquisitions are also reported surface is assumed to undergo melt is -0.0158, and is shown as dashed horizontal line in the right panels each plot.

### 3.2 Coherence analysis

The coherence time series show a completely different behaviour than the NRCS- $\sigma^0$  time series (Fig. 3). On the Amery ice shelf Ice Shelf, for example, snow, ice and lakes all have low or null coherence in summer, because of the altering scattering properties due to melt water content. For the ice and snow zones, the coherence rises abruptly when the surface refreezes in spring, while the coherence over the lakes rises only gradually until winter, when the lakes reach coherence values that are similar to snow and ice. During winter, the coherence levels from snow, ice and lakes show a similar behaviour with large temporal variations when the coherence suddenly drops (i.e. fluctuating between 0.2 and 0.8 on 6 day time spans). These sudden drops are probably due to weather-induced changes in scattering properties (e.g. after a snowfall event), as shown in panel a) of Fig. 5). These drops are however sparse as the 6-day revisit cycle allows to get good overall coherence.

On RBIS, on the other hand, the coherence is lower as the Sentinel-1 data are only available in a 12-day revisit cycle, which reduces the overall coherence and makes interpretation more complicated as more weather-induced changes in scattering properties could occur in a 12-day revisit. Panel b) of Fig. 5, for example, shows that region R1 (on RBIS) has stronger

precipitation than region A2 (on Amery). Despite the overall lower coherence, ~~also on RBIS~~ the coherence time series on  
220 RBIS also show a relatively stable period from August to October, with coherence values above 0.35. From Nov. 2016 to Jan.  
Between Oct. 2017 and Jan. 2018, the coherence drops drastically, with an almost null coherence for all polygons surveyed  
snow, ice and lake areas. The coherence then increases again ~~when the snow and ice surfaces refreeze~~ in February. Overall,  
snow reaches the highest coherence (0.5-~~0.6~~-0.6), while the lakes show the lowest coherence. ~~Lakes RBIS a and RBIS f~~  
~~however showed significant coherence values (0.4) during the winter season (only occasionally for RBIS a), while RBIS g~~  
225 ~~presented null values throughout the whole year. This difference in behaviour could indicate differences in refreezing status.~~

To better understand the ~~NRCS and coherence times~~  $\sigma^0$  and coherence time series, some representative lake features in the  
Amery and RBIS zones are analysed in more detail in Fig. 7 and Fig. 8. The outlined lakes on Amery Ice Shelf in Fig. 7 are  
characterised by dominant blue ice cover with low backscatter intensities, as conveyed by the dark background in the ~~NRCS~~  $\sigma^0$   
panels. The ice-blue ice region is intermittently covered by a shallow snow layer (e.g. Landsat RGB image of Oct. 2017 )~~which~~  
230 ~~melts away in Fig. 7) which decreases~~ in summer (e.g. Landsat RGB image of Jan. 2018 in Fig. 7). This results in a stable  
ice surface with high coherence values. The lakes, on the other hand, show a more variable behaviour with lower coherence  
and strong changes in ~~NRCS~~  $\sigma^0$  as a result of varying scattering properties. At the end of the summer (Mar. 2017), both lakes  
show a low ~~NRCS~~  $\sigma^0$  whereas it becomes substantially brighter-greater in the subsequent acquisitions from July to Nov. 2017.  
~~This corresponds to the observed NRCS increase Apr. 2017 for Amery b in Fig. 3. The NRCS and coherence signal is~~  $\sigma^0$  and  
235 ~~coherence are~~ moreover not uniform across each lake with the appearance of polygonal features that show large differences  
between the centre of the lake (with higher ~~NRCS~~  $\sigma^0$  and coherence) and a thin strip at the edges (with lower ~~NRCS~~  $\sigma^0$  and  
coherence). This is consistent with earlier observations based on optical satellite imagery, where the lakes show a circular  
appearance with a thick snow/ice lid in the ~~center-centre~~ and ice/water at the edges (e.g., Fig. S1 in Dunmire et al., 2020). This  
pattern often changes over time~~as for example, for example, as~~ in the lake Amery c (Fig. 7), where the coherence increases for  
240 half of the lake and not for the other half, which could be an indicator of gradual~~non-spatially uniform, spatially non-uniform~~  
refreezing or drainage. One example of such a drainage event could be seen in the small circular feature in the coherence of  
Amery b in Nov. 2017 (indicated by the arrow in the Nov. 2017 coherence image of Fig. 7), which clearly corresponds to a  
collapsed circular feature in the Jan. 2018 Landsat imagery. Moreover, between Amery b and c, a hydrological network that  
is clearly visible as high  $\sigma^0$  in the  $\sigma^0$  panels is present only in the Mar. 2017 coherence panel as low coherence. This could  
245 suggest the surface refreezing between Mar. and Jul. 2017, similar to that discussed by Antonova et al. (2016).

On RBIS, the lakes are located in an area that contains both snow/firm ~~regions region~~ and blue ice. ~~Since (Lenaerts et al., 2016)~~  
. Differently from data on Amery Ice Shelf, the Sentinel-1 SLC ~~temporal coverage is lower than for Amery, SLC coverage~~  
acquisition only started in July 2017, with a 12-day revisit (Fig. 8). ~~The lake-Lake~~ RBIS a shows a high ~~NRCS~~  $\sigma^0$  in October  
and a low ~~NRCS~~  $\sigma^0$  in February, which contrasts with the surroundings. The other lakes show a smaller contrast with their  
250 surroundings with ~~intermediate NRCS only intermediate~~  $\sigma^0$  values. The whole area frequently ~~underwent undergoes~~ coherence  
losses, especially ~~in winter between Nov. 2017 and Jan. 2018~~ (Fig. 3d), ~~possibly due to the 12-day revisit time.~~ In Fig. 5, panel  
b) shows that precipitation may cause the drop in coherence, as in Oct.-Nov. 2017 it is 2-5 times higher than in other times.  
Panel c) of Fig. 6 shows that the low coherence between Dec. 2017 and Jan. 2018 may be caused by melt, as the XPGR values

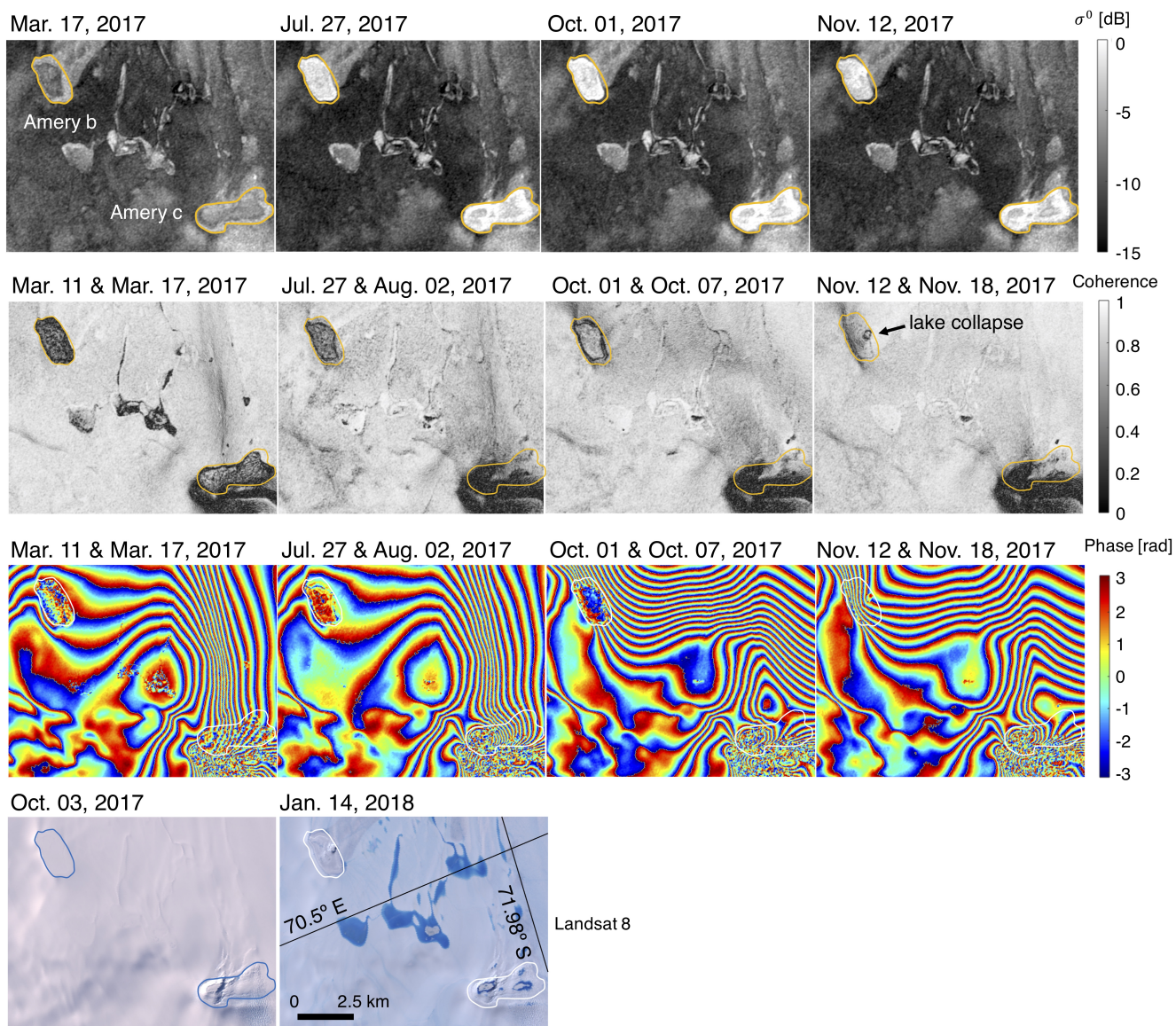


**Figure 7.** Outline for two lakes of interest on Amery Ice Shelf (referred to as Amery b and c in Fig. 1).  $\sigma^0$ , coherence and resulting phase difference interferograms are shown for four representative dates throughout the year. The high frequency fringes surrounding each lake represent a convolution of both ice flow and tidal motion. Two Landsat RGB images are also shown to aid the visual interpretation of the radar features.

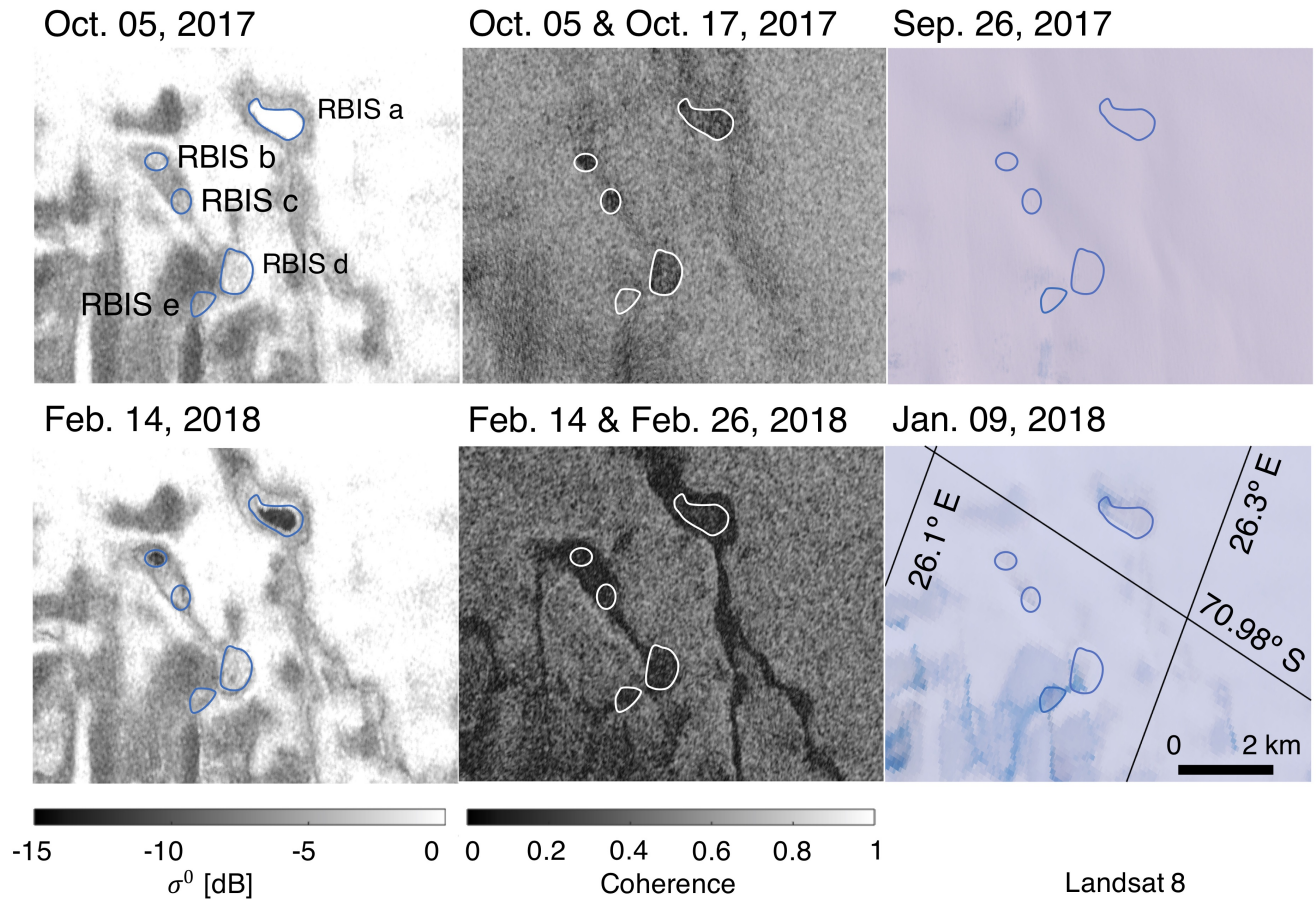


**Figure 8.** Coherence and  $\sigma^0$  in the RBIS region before (upper panels) and during (lower panels) the surface melt in the vicinity of RBIS a in the panels R1 of Fig. 1. These lakes are hereafter referred to as RBIS a to e. Two cloud-free Landsat RGB images close to the radar acquisitions are also shown (right panels).

during this period exceed the melting threshold. In Oct. 2017 and Feb. 2018, however, coherence is higher ( $>0.35$ , see both Fig. 3 and Fig. 8). In both coherence image pairs in Fig. 8, the meltwater features, with low or null coherence values, are sharply emerging from the background. In Feb. 2018, the coherence pairs moreover highlight a hydrological connection between the lakes, which is shown as dark strips between the highlighted lakes in the lower middle panel of Fig. 8. The patterns are clearly newly formed compared to the Oct. 2017 coherence panel of Fig. 8. This change is not straightforward to see in the NRCS- $\sigma^0$  or optical imagery. This highlights the increased potential for coherence over the backscatter intensity in delineating the lake network.

### 3.3 Interferogram analysis

~~The interferogram phases~~ Interferometric phase difference maps (Fig. 7) emphasise the differences in spatial cover and melting patterns between the two lakes on Amery ~~ice shelf~~ Ice Shelf. The centre of lake Amery b shows low-frequency fringes in all the acquisitions, even in March, despite the relatively low coherence. Between Mar. 2017 and Oct. 2017 ~~the fringes are however~~, the fringes in the centre of lake Amery b are disconnected from the high-frequency fringes of the surroundings, whereas they connect seamlessly in ~~November~~ Nov. 2017. This pattern of discontinuity is consistent with lower coherence at the edges ~~of lake Amery b, which follows the orange delineation curve in the Oct. 2017 coherence panel of Fig. 7~~. Both the fringe discontinuity and coherence increase ~~between Oct. and Nov. through time~~ indicate the presence of ~~meltwater the lake~~ until Oct. 2017, followed by a lake refreeze or drainage in ~~Nov. The November of that year~~. Consistent with our InSAR-based observations, Landsat images show a smooth ~~snow-covered~~ snow-covered surface in Oct. 2017 and a rough doline-like surface in Jan. ~~2018–2018 (labelled as lake collapse in the coherence panel of Fig. 7)~~. This supports the hypothesis that the lake drained and the surface collapsed, and highlights the potential of coherence and interferogram ~~analysis~~ for analysing meltwater dynamics.

On the eastern part of RBIS, the interferogram shows a different potential for analysing meltwater dynamics (Fig. 9) as it shows a phase reversal from right to left of the Dec. 2017 phase image (i.e. ~~reversing the colour scheme in the interferogram panels) over the lake area in Dec. 2017 vs.~~ fringes change from red–blue–green–yellow to red–yellow–green–blue, forming a whirl-like feature) compared to a continuous phase ~~in Apr. 2018. from right to left of the Apr. 2018 image (i.e. fringes are constantly red–yellow–green–blue)~~. This phase reversal indicates that the lake has a displacement in the satellite line-of-sight which is opposite to the rest of the ice shelf. As the ice shelf background fringes correspond to the ice flow and presumably tidal component, in this case moving away from the satellite line-of-sight, the lake fringes indicate an uplift as a result of ice shelf rebound after lake collapse. This would be consistent with rebound effects as described in Banwell et al. (2013). Indirect indicators of this lake collapse can also be observed in the Landsat 8 images before/after the collapse, as the roughness of the surface strongly increased after the collapse.

Another potential of interferogram time series is the detection of lake refreezing, as can be observed for the large lake feature in the middle of ~~the Amery~~ Amery Ice Shelf, labelled as Amery a in Fig. 1. Both Amery a and the surrounding ice shelf show an overall low NRCS- $\sigma^0$  and a complete incoherent interferogram on Jan. 4, 2017 (Fig. 10) as a result of surface melt. In subsequent weeks ~~the NRCS-, the  $\sigma^0$~~  and coherence of the snow surrounding area increase due to the refreezing, as can be seen from the visible regular fringes. For the lake, however, this increase in coherence lags behind and only recovers slowly as more portions of the lake start to refreeze. During the refreezing, the fringes patterns over the lake gradually recover while the incoherent noise gradually diminishes. Both the Landsat panels of Fig. 10 and panel a) of Fig. 5 show that Jan. 2017 is a more intense melt season than Jan. 2018, which is consistent to the observation from the fringes. This pattern corresponds closely with the refreezing pattern identified by (Spergel et al., 2021) who also identified a gradual refreezing ~~starting at the edges towards the centre of the lake~~ over 66 days based on transition from high-to-low backscatter intensity only. The interferogram shows similar results here, ~~but with the added value that the interpretation of high-low backscatter compared to the surroundings is less ambiguous~~. However, compared to interpreting the refreezing of the lake solely based on backscatter intensity, adding interferograms to the observation helps reduce ambiguities in the interpretation.



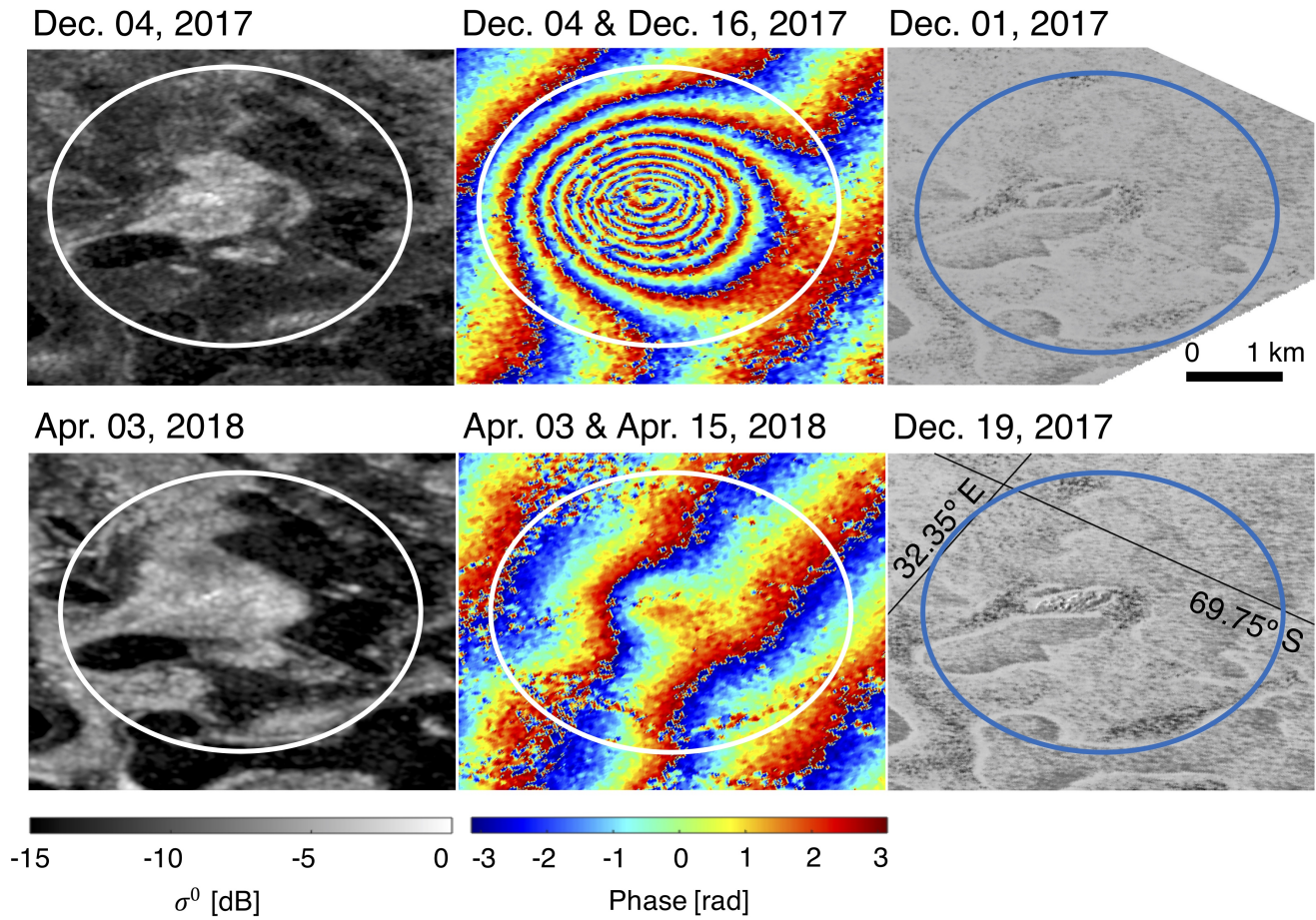


**Figure 9.** NRCS- $\sigma^0$  and interferogram phases-interferograms for a lake feature in the east of the RBIS experiencing drainage in December 2017 (left-upper panels) and ice-cover collapse in April 2018 (centre-lower panels). Two near-contemporaneous Landsat 8 panchromatic (band 8) images in-correspondence-of-the-two-events are also shown (right panels).

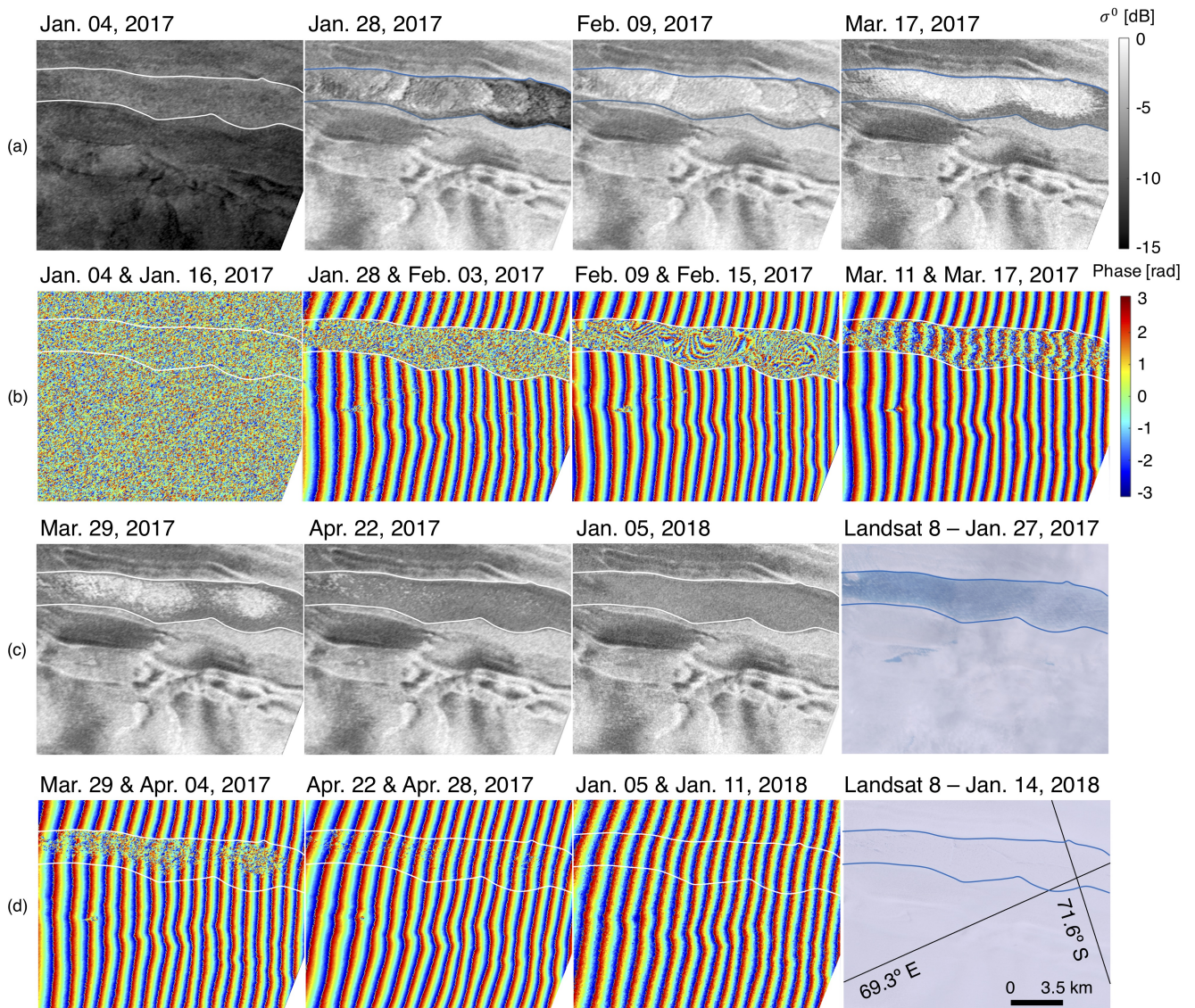


**Figure 10.**  $\text{NRCS-}\sigma^0$  and interferogram-phases-interferograms for a large lake in the middle of the Amery region experiencing a refreezing process. The  $\text{NRCS-}\sigma^0$  refers to the first image of the interferogram pairs. The interferograms clearly show that the lake refreezing occurs in the first half of 2017. The lake remains frozen throughout the remainder of 2017 and in 2018. The two Landsat 8 RGB images in the lower right corner provide a visual evaluation.

## 4 Discussion

~~The different case studies provide an overview of the potential and shortcomings~~ Using SAR-based observations acquired across two East Antarctic ice shelves, this study presents evidence of the utility of backscatter intensity and coherence to assess meltwater lake dynamics. Low backscatter intensities can indicate blue ice areas or strong absorption due to meltwater, while high backscatter intensities indicate rough surfaces or strong volume scattering due to larger refrozen snow grains. ~~The~~ Moreover, the partly frozen lakes ~~show moreover often often show~~ a bright centre (high  $\text{NRCS}\sigma^0$ ) that can be attributed to the single bounce mechanism at the rough ~~ice-water ice-water~~ boundary (Engram et al., 2013; Atwood et al., 2015; Antonova et al., 2016). Due to this contrasting behaviour, the identification and characterisation of the meltwater features only based on backscatter intensity is not straightforward. Several of the observed lakes ~~show for examplesimilar NRCS as their surrounding~~ , for example, show  $\sigma^0$  similar to their surroundings for long periods, and even during the freezing/melting processes (e.g. Fig. 8 ~~or and~~ Fig. 10).

Backscatter intensity therefore may not be sufficient to fully characterise meltwater processes. ~~Coherence~~ Interferometric coherence, however, provides additional dynamic information as it helps ~~assessing assess~~ the degree of stability of the ice cover between two acquisitions. Coherence is an important property estimated from interferometric computation of ~~Sentinel-1~~ SLC data. For repeat-pass acquisition ~~such as Sentinel-1~~, a loss of coherence mainly reveals the extent of a surface change (Zebker and Villasenor, 1992). However, with substantial microwave penetration depths in snow/firn, coherence variations indicate changes in scattering properties. Coherence losses consequently may be due to changes in volume scattering (Zebker and Hoen, 2000) or subsurface processes. Low coherence between interferometric images can therefore indicate altering scattering properties (e.g. a strong snowfall or an intense melt event), but also changes in ~~ice-water ice-water~~ interface due to refreezing meltwater lakes (Antonova et al., 2016) where refreezing may result in a ~~gradually gradual~~ increase in coherence. Ice and snow areas are typically characterised by a high coherence, while meltwater lakes show a low coherence due to the constantly changing ~~ice/water interface ice-water interface and the increased attenuation due to the presence of water~~. This added value of coherence is shown, for example, in Fig. 7 and 8, where ~~the~~ coherence provides more insight into the temporal dynamics of the lakes than the  $\text{NRCS}\sigma^0$  images alone. The change from ~~disk-shaped disk-shaped~~ low coherence patterns to ~~ring-shaped ring-shaped~~ patterns (Fig. 7) ~~for example provide~~, for example, provides an important indicator of the gradual refreezing patterns (i.e. more refreezing in the centre than at the edges). These results correspond to the study of Antonova et al. (2016), where the melting and refreezing of lake ice could be observed by using both backscatter intensity and coherence image time series.

~~Also the interferometric phase has shown to be a useful indicator~~ Beyond coherence, we also demonstrate the potential of interferometric phase for assessing meltwater dynamics ~~when the interferometric images show a in areas of~~ high coherence. ~~Local volume changes caused by gradual refreezing may be hard to quantify because the refreezing process may change the ice-water interface constantly, affecting the quality of the interferogram. However, the~~ For example, the deformation due to ~~instant rapid~~ meltwater events, such as drainage and collapse, may be captured, if the fringe pattern in the lake area appears highly distinct to the surroundings affected by tidal ~~displacement and horizontal motion~~. Within this context, we ~~identified~~

identify two advantages of the phase fringes over the NRCS- $\sigma^0$  and coherence alone: i) an easier detection of stable ice or refrozen and lake refreezing than coherence and backscatter intensity and ii) the detection of relative motion related due to uplift and subsidence events as a result of lake drainage or lake filling. The first advantage is clear in Figs. 7–10, where the phase patterns allow additional interpretation of the refreezing patterns which cannot be revealed by the coherence or backscatter intensity alone. The second advantage is in Fig. 9, where we could estimate the presence of a uplift event due to lake drainage.

Although the InSAR analysing approach shows a While InSAR-based techniques show clear potential for assessing meltwater lake dynamics, it also comes with challenges and drawbacks monitoring meltwater lake evolution, there are several key limitations associated with this technique compared with conventional optical- and SAR backscatter-based imaging. First, it requires high coherence between image pairs to allow a meaningful interpretation of meltwater lake dynamics (e.g. as in Fig. 10). When the revisit cycle for SLC data is low long or when the surface changes due to other processes (e.g. strong snow-fall event), as in Fig. 5) are frequent, the interpretation of coherence and phase changes may can be limited. On Amery Ice Shelf, the Sentinel-1 mission has a 6-day revisit, whilst the revisit period on the RBIS is 12 day. Due to this difference days. The amount of precipitation is also lower on Amery Ice Shelf compared to RBIS. Due to these differing imaging times and weather, the lake processes are better observed on Amery than the Ice Shelf than RBIS. Second, the interpretation of phase change can only should be done relative to the displacement of the lake surroundings in the line-of-sight. As For example, as the meltwater lakes typical develop on typically develop in locations with strong ice and/or tidal displacement, interpretation should be done relative to that displacement which makes interpretation more complicated. Therefore, to better derive the exact height change of lake ice lids, additional processing is needed to cancel out ice movements (Mohajerani et al., 2021) and to filter out signals due to tidal movements (McMillan et al., 2012). With SAR acquisitions from sensors in both ascending and descending orbits, it is however possible to better quantify the lake subsidence/uplift.

A potential improvement of lake monitoring using InSAR is the launch of new satellite missions. The launch of Sentinel-1C (Torres et al., 2017), for example, can provide <6-day imaging capabilities to improve coherence of the ice and snow surface. The launch of the NASA-ISRO SAR (NISAR) mission, moreover, provides L-band and S-band repeat-pass interferometry with the repeat cycle of 12 days (Rosen et al., 2017). The long wavelength of this mission has the potential to measure deeper lake dynamics and to circumvent drifting snow and other atmospheric effects.

## 5 Conclusions

The goal of this study was to provide an insight on the capabilities of coherent and incoherent SAR data to assess the meltwater This study has provided insights into the utility of InSAR for monitoring meltwater lake dynamics on ice shelves. Four regions with intense melt on two ice shelves in Antarctica have been analysed based on C-band Sentinel-1 SAR data and Sentinel-1A/B SAR data, corresponding available Landsat 8 imagery, ERA5 precipitation data and SSMIS brightness temperature data. The spatial and temporal inspection of the meltwater features conveyed that the conveys that backscatter intensity allows identification of the freezing and melting events, as the lakes show an increase of the backscatter intensity due to the water-ice

water-ice boundary when the lake is not completely frozen. The extent of such dynamics ~~however~~ depends on the morphol-  
365 ogy of the lake and on the weather conditions. ~~A generalisation on of the meltwater detection is however not straightforward~~  
We show that meltwater detection using backscatter is, however, not straightforward, as meltwater lakes often show similar  
backscatter intensity values to their surroundings. In such ~~context~~circumstance, InSAR information ~~, i.e. the coherence and the~~  
~~interferogram phases,~~ can be useful to increase the confidence of such delineation, especially during the freezing and melting  
period. ~~Besides, such indicators can be additionally exploited to infer the stability of the lake ice and its connection with the~~  
370 ~~ice layer in the ground. The coherence in this context allows to detect~~In addition, we show that InSAR-derived information  
can also be used to observe meltwater lake evolution (and potential drainage) with high accuracy beyond that afforded by  
conventional backscatter or optical satellite imaging. Specifically, InSAR coherence information allows for the detection of  
changes in the ~~ice-water interface~~ice-water interface, which shows clearer patterns than the backscatter intensity alone, while  
~~the interferograms can reveal refreezing patterns. The interferograms allow moreover to detect the relative displacement of~~  
375 ~~the lakes which can be useful to detect~~interferometric phase can effectively track the spatial and temporal evolution of ice  
refreezing. Maps of interferometric phase moreover allow for the detection of abrupt lake drainage ~~or filling~~(or filling) events  
via changes in the relative displacement of the surface between successive SAR passes.

~~The paper also points at the limitations that due to the 12 days~~Despite noted limitations to current Sentinel-1 ~~repeat eye~~  
~~over the RBIS, is it hardly sufficient to provide an inter-annual observation and comparison. A revisit larger than 6 days may~~  
380 ~~greatly reduce the coherence and compromise the quality of the (complicated) unwrapping step over the ice shelf. Several~~  
~~InSAR products completely impaired by weather events, in winter, most likely attributable to precipitations and wind, and by~~  
~~fast surface changes in summer, were found as a result.~~

~~In conclusion, InSAR imaging over parts of Antarctica,~~ this study shows ~~a promising possibility to monitor the local~~  
~~dynamics of specific water features on the ice shelves by using InSAR, potentially paving the way towards that InSAR provides~~  
385 promising potential for monitoring meltwater lake dynamics beyond that afforded by conventional, backscatter-only, analyses.  
Such potential could pave the way for dedicated Sentinel-1 meltwater products that could facilitate the study of ice shelves in  
a changing climate.

*Code availability.* The DORIS software used to process Sentinel-1 SLC data is available at <http://doris.tudelft.nl>.

*Data availability.* The TanDEM-X data used for geo-coding the InSAR SLC products on the RBIS are available at [https://doi.org/10.1594/](https://doi.org/10.1594/pangaea.868109)  
390 [pangaea.868109](https://doi.org/10.1594/pangaea.868109).

*Author contributions.* SL developed the idea of this study and provided access to the mapped locations of the meltwater ponds on the  
RBIS and TanDEM-X data. PLD provided expertise in processing and interpreting InSAR data. WL was responsible for managing the data,

processing the data with DORIS, generating melt extent and precipitation time series, processing and analysing the results, producing the figures, and providing the manuscript.

395 *Competing interests.* The authors declare they have no conflict of interest.

*Acknowledgements.* We are grateful for the DORIS development team at TU Delft. We acknowledge Copernicus Open Access Hub for providing Sentinel-1 SLC data, and Google Earth Engine for providing Landsat 8 and Sentinel-1 GRD images. [This study contains modified Copernicus Climate Change Service information.](#)

400 DEM for visualisation is provided by the Byrd Polar and Climate Research Center and the Polar Geospatial Center under NSF-OPP awards 1543501, 1810976, 1542736, 1559691, 1043681, 1541332, 0753663, 1548562, 1238993 and NASA award NNX10AN61G. Computer time is provided through a Blue Waters Innovation Initiative. The DEM is produced using data from DigitalGlobe, Inc.

We would also like to thank Dr Lorenzo Iannini and Malte Manne for proof-reading and discussion. [Additional thanks to the Referees for reviewing the manuscript.](#)

## References

- 405 Abdalati, W. and Steffen, K.: Passive microwave-derived snow melt regions on the Greenland Ice Sheet, *Geophysical Research Letters*, 22, 787–790, <https://doi.org/https://doi.org/10.1029/95GL00433>, 1995.
- Antonova, S., Duguay, C., Käab, A., Heim, B., Langer, M., Westermann, S., and Boike, J.: Monitoring Bedfast Ice and Ice Phenology in Lakes of the Lena River Delta Using TerraSAR-X Backscatter and Coherence Time Series, *Remote Sensing*, 8, 903, <https://doi.org/10.3390/rs8110903>, 2016.
- 410 Atwood, D. K., Gunn, G. E., Roussi, C., Wu, J., Duguay, C., and Sarabandi, K.: Microwave Backscatter From Arctic Lake Ice and Polarimetric Implications, *IEEE Transactions on Geoscience and Remote Sensing*, 53, 5972–5982, <https://doi.org/10.1109/TGRS.2015.2429917>, 2015.
- Banwell, A. F., MacAyeal, D. R., and Sergienko, O. V.: Breakup of the Larsen B Ice Shelf triggered by chain reaction drainage of supraglacial lakes, *Geophysical Research Letters*, 40, 5872–5876, <https://doi.org/10.1002/2013gl057694>, 2013.
- 415 Bell, R. E., Banwell, A. F., Trusel, L. D., and Kingslake, J.: Antarctic surface hydrology and impacts on ice-sheet mass balance, *Nature Climate Change*, 8, 1044–1052, <https://doi.org/10.1038/s41558-018-0326-3>, <http://www.nature.com/articles/s41558-018-0326-3>, 2018.
- Benedek, C. L. and Willis, I. C.: Winter drainage of surface lakes on the Greenland Ice Sheet from Sentinel-1 SAR imagery, *The Cryosphere*, 15, 1587–1606, <https://doi.org/10.5194/tc-15-1587-2021>, 2021.
- Brucker, L., Picard, G., and Fily, M.: Snow grain-size profiles deduced from microwave snow emissivities in Antarctica, *Journal of Glaciology*, 56, 514–526, <https://doi.org/10.3189/002214310792447806>, 2010.
- 420 Chander, G., Markham, B. L., and Helder, D. L.: Summary of current radiometric calibration coefficients for Landsat MSS, TM, ETM+, and EO-1 ALI sensors, *Remote Sensing of Environment*, 113, 893–903, <https://doi.org/https://doi.org/10.1016/j.rse.2009.01.007>, 2009.
- Copernicus: Open Access Hub, <https://scihub.copernicus.eu>, [accessed 28 Apr. 2018], 2014.
- Copernicus Climate Change Service (C3S): ERA5: Fifth generation of ECMWF atmospheric reanalyses of the global climate, Copernicus Climate Change Service Climate Data Store (CDS), <https://cds.climate.copernicus.eu/cdsapp#!/home>, [accessed Oct. 13, 2021], 2017.
- 425 De Zan, F. and Monti Guarnieri, A.: TOPSAR: Terrain Observation by Progressive Scans, *IEEE Transactions on Geoscience and Remote Sensing*, 44, 2352–2360, <https://doi.org/10.1109/tgrs.2006.873853>, 2006.
- Dirscherl, M., Dietz, A. J., Kneisel, C., and Kuenzer, C.: A Novel Method for Automated Supraglacial Lake Mapping in Antarctica Using Sentinel-1 SAR Imagery and Deep Learning, *Remote Sensing*, 13, <https://doi.org/10.3390/rs13020197>, 2021.
- 430 Dunmire, D., Lenaerts, J. T. M., Banwell, A. F., Wever, N., Shragge, J., Lhermitte, S., Drews, R., Pattyn, F., Hansen, J. S. S., Willis, I. C., Miller, J., and Keenan, E.: Observations of Buried Lake Drainage on the Antarctic Ice Sheet, *Geophysical Research Letters*, 47, e2020GL087970, <https://doi.org/https://doi.org/10.1029/2020GL087970>, 2020.
- Engram, M., Anthony, K. W., Meyer, F. J., and Grosse, G.: Characterization of L-band synthetic aperture radar (SAR) backscatter from floating and grounded thermokarst lake ice in Arctic Alaska, *The Cryosphere*, 7, 1741–1752, <https://doi.org/10.5194/tc-7-1741-2013>, 435 2013.
- Fahnestock, M., Bindschadler, R., Kwok, R., and Jezek, K.: Greenland Ice Sheet Surface Properties and Ice Dynamics from ERS-1 SAR Imagery, *Science*, 262, 1530–1534, <https://doi.org/10.1126/science.262.5139.1530>, 1993.
- Gerrish, L., Fretwell, P., and Cooper, P.: Medium resolution vector polylines of the Antarctic coastline, <https://doi.org/10.5285/824B5350-763E-4933-BB76-09F5D24CB033>, 2021.
- 440 Hanssen, R. F.: *Radar Interferometry*, Springer Netherlands, <https://doi.org/10.1007/0-306-47633-9>, 2001.

- Hillebrand, F. L., de Carvalho Barreto, I. D., Bremer, U. F., Arigony-Neto, J., Mendes Júnior, C. W., Simões, J. C., da Rosa, C. N., and de Jesus, J. B.: Application of textural analysis to map the sea ice concentration with sentinel 1A in the western region of the Antarctic Peninsula, *Polar Science*, p. 100719, <https://doi.org/https://doi.org/10.1016/j.polar.2021.100719>, 2021.
- 445 Hirose, T., Kapfer, M., Bennett, J., Cott, P., Manson, G., and Solomon, S.: Bottomfast Ice Mapping and the Measurement of Ice Thickness on Tundra Lakes Using C-Band Synthetic Aperture Radar Remote Sensing, *JAWRA Journal of the American Water Resources Association*, 44, 285–292, <https://doi.org/10.1111/j.1752-1688.2007.00161.x>, 2008.
- Howat, I. M., Porter, C., Smith, B. E., Noh, M.-J., and Morin, P.: The Reference Elevation Model of Antarctica, *The Cryosphere*, 13, 665–674, <https://doi.org/10.5194/tc-13-665-2019>, 2019.
- Johnson, A., Fahnestock, M., and Hock, R.: Evaluation of passive microwave melt detection methods on Antarctic Peninsula ice shelves using 450 time series of Sentinel-1 SAR, *Remote Sensing of Environment*, 250, 112 044, <https://doi.org/https://doi.org/10.1016/j.rse.2020.112044>, 2020.
- Kingslake, J., Ely, J. C., Das, I., and Bell, R. E.: Widespread movement of meltwater onto and across Antarctic ice shelves, *Nature*, 544, 349–352, <https://doi.org/10.1038/nature22049>, 2017.
- Kunkee, D. B., Poe, G. A., Boucher, D. J., Swadley, S. D., Hong, Y., Wessel, J. E., and Uliana, E. A.: Design and Evaluation 455 of the First Special Sensor Microwave Imager/Sounder, *IEEE Transactions on Geoscience and Remote Sensing*, 46, 863–883, <https://doi.org/10.1109/tgrs.2008.917980>, 2008.
- Lenaerts, J. T. M., Lhermitte, S., Drews, R., Ligtenberg, S. R. M., Berger, S., Helm, V., Smeets, C. J. P. P., van den Broeke, M. R., van de Berg, W. J., van Meijgaard, E., Eijkelboom, M., Eisen, O., and Pattyn, F.: Meltwater produced by wind–albedo interaction stored in an East Antarctic ice shelf, *Nature Climate Change*, 7, 58–62, <https://doi.org/10.1038/nclimate3180>, 2016.
- 460 McMillan, M., Shepherd, A., Gourmelen, N., Park, J.-W., Nienow, P., Rinne, E., and Leeson, A.: Mapping ice-shelf flow with interferometric synthetic aperture radar stacking, *Journal of Glaciology*, 58, 265–277, <https://doi.org/10.3189/2012jog11j072>, 2012.
- Miles, K. E., Willis, I. C., Benedek, C. L., Williamson, A. G., and Tedesco, M.: Toward Monitoring Surface and Subsurface Lakes on the Greenland Ice Sheet Using Sentinel-1 SAR and Landsat-8 OLI Imagery, *Frontiers in Earth Science*, 5, <https://doi.org/10.3389/feart.2017.00058>, 2017.
- 465 Mohajerani, Y., Jeong, S., Scheuchl, B., Velicogna, I., Rignot, E., and Milillo, P.: Automatic delineation of glacier grounding lines in differential interferometric synthetic-aperture radar data using deep learning, *Scientific Reports*, 11, <https://doi.org/10.1038/s41598-021-84309-3>, 2021.
- Nagler, T., Rott, H., Ripper, E., Bippus, G., and Hetzenecker, M.: Advancements for Snowmelt Monitoring by Means of Sentinel-1 SAR, *Remote Sensing*, 8, <https://doi.org/10.3390/rs8040348>, 2016.
- 470 Nikaein, T., Iannini, L., Molijn, R. A., and Lopez-Dekker, P.: On the Value of Sentinel-1 InSAR Coherence Time-Series for Vegetation Classification, *Remote Sensing*, 13, <https://doi.org/10.3390/rs13163300>, <https://www.mdpi.com/2072-4292/13/16/3300>, 2021.
- Prats-Iraola, P., Scheiber, R., Marotti, L., Wollstadt, S., and Reigber, A.: TOPS Interferometry With TerraSAR-X, *IEEE Transactions on Geoscience and Remote Sensing*, 50, 3179–3188, <https://doi.org/10.1109/TGRS.2011.2178247>, 2012.
- Rizzoli, P., Martone, M., Rott, H., and Moreira, A.: Characterization of Snow Facies on the Greenland Ice Sheet Observed by TanDEM-X 475 Interferometric SAR Data, *Remote Sensing*, 9, <https://doi.org/10.3390/rs9040315>, 2017.
- Rosen, P. A., Kim, Y., Kumar, R., Misra, T., Bhan, R., and Sagi, V. R.: Global persistent SAR sampling with the NASA-ISRO SAR (NISAR) mission, in: 2017 IEEE Radar Conference (RadarConf), pp. 0410–0414, <https://doi.org/10.1109/RADAR.2017.7944237>, 2017.



- Selmes, N., Murray, T., and James, T. D.: Characterizing supraglacial lake drainage and freezing on the Greenland Ice Sheet, *The Cryosphere Discussions*, 7, 475–505, <https://doi.org/10.5194/tcd-7-475-2013>, 2013.
- 480 Spergel, J. J., Kingslake, J., Creyts, T., van Wessem, M., and Fricker, H. A.: Surface meltwater drainage and ponding on Amery Ice Shelf, East Antarctica, 1973–2019, *Journal of Glaciology*, p. 1–14, <https://doi.org/10.1017/jog.2021.46>, 2021.
- Torres, R., Snoeij, P., Geudtner, D., Bibby, D., Davidson, M., Attema, E., Potin, P., Rommen, B., Floury, N., Brown, M., Traver, I. N., Deghaye, P., Duesmann, B., Rosich, B., Miranda, N., Bruno, C., L'Abbate, M., Croci, R., Pietropaolo, A., Huchler, M., and Rostan, F.: GMES Sentinel-1 mission, *Remote Sensing of Environment*, 120, 9–24, <https://doi.org/10.1016/j.rse.2011.05.028>, 2012.
- 485 Torres, R., Lokas, S., Di Cosimo, G., Geudtner, D., and Bibby, D.: Sentinel 1 evolution: Sentinel-1C and -1D models, in: 2017 IEEE International Geoscience and Remote Sensing Symposium (IGARSS), pp. 5549–5550, <https://doi.org/10.1109/IGARSS.2017.8128261>, 2017.
- Ulaby, F. T., Moore, R. K., and Fung, A. K.: *Microwave Remote Sensing Active and Passive*, The Artech House Remote Sensing Library, 1981.
- 490 Williamson, A. G., Arnold, N. S., Banwell, A. F., and Willis, I. C.: A Fully Automated Supraglacial lake area and volume Tracking (“FAST”) algorithm: Development and application using MODIS imagery of West Greenland, *Remote Sensing of Environment*, 196, 113–133, <https://doi.org/10.1016/j.rse.2017.04.032>, 2017.
- Yague-Martinez, N., Prats-Iraola, P., Rodriguez-Gonzalez, F., Brcic, R., Shau, R., Geudtner, D., Eineder, M., and Bamler, R.: Interferometric Processing of Sentinel-1 TOPS Data, *IEEE Transactions on Geoscience and Remote Sensing*, 54, 2220–2234, <https://doi.org/10.1109/tgrs.2015.2497902>, 2016.
- 495 Yague-Martinez, N., De Zan, F., and Prats-Iraola, P.: Coregistration of Interferometric Stacks of Sentinel-1 TOPS Data, *IEEE Geoscience and Remote Sensing Letters*, PP, 1–5, <https://doi.org/10.1109/LGRS.2017.2691398>, 2017.
- Zebker, H. and Hoen, E. W.: Penetration depths inferred from interferometric volume decorrelation observed over the Greenland Ice Sheet, *IEEE Transactions on Geoscience and Remote Sensing*, 38, 2571–2583, <https://doi.org/10.1109/36.885204>, 2000.
- 500 Zebker, H. and Villasenor, J.: Decorrelation in interferometric radar echoes, *IEEE Transactions on Geoscience and Remote Sensing*, 30, 950–959, <https://doi.org/10.1109/36.175330>, 1992.